Amphiphilic Multiblock Copolymers: From Intramolecular Pearl Necklace to Layered Structures

Virginie Hugouvieux* and Monique A. V. Axelos

INRA, UR1268 Biopolymères Interactions Assemblages, F-44300 Nantes, France

Max Kolb

Laboratoire de Chimie, Ecole Normale Supérieure de Lyon, 46, allée d'Italie, F-69364 Lyon cedex 7, France

Received April 3, 2008; Revised Manuscript Received September 3, 2008

ABSTRACT: We report on three-dimensional Monte Carlo simulations of dilute solutions of multiblock copolymers made of regularly spaced hydrophobic and hydrophilic blocks in the limit of long chains with a large number of blocks. Using a lattice model we investigate the effects of the ratio of hydrophobic to hydrophilic block lengths and impact of the quality of the solvent on the intramolecular structure of the copolymers. In poor solvent and for given block lengths the simulations show evidence for the existence of different kinds of intramolecular self-assemblies depending on solvent quality: Micelles, chains of micelles, tubes, and layered structures are revealed by both statistical properties and visualization. The form factor signature of the different structures has been identified and is discussed in connection with its experimental observability. The existence region of the different conformations in terms of energy and entropy is summarized in a phase diagram.

I. Introduction

Amphiphilic copolymers have attracted much interest for many years because they have a dual affinity to their environment: these copolymers consist of covalently bound polar and apolar monomers which behave differently in solution and at interfaces. Due to this dual property with respect to their environment, amphiphilic copolymers self-organize, both in solution and at interfaces, in order to minimize their free energy. This leads to self-assemblies with well-defined morphologies, from microphase separation in solution to self-organization at and stabilization of interfaces.[1] These properties make amphiphilic copolymers useful in many industrial applications as stabilizers in the formation of nanoparticles, as rheology modifiers in formation of gels, as emulsifiers, or as wetting agents.[2,3] In the past decade the biomedical application of amphiphilic block copolymers with biocompatible sequences have been widely extended in drug delivery systems[4] or for preparing injectable scaffold materials for tissue engineering.[5] There exist many different kinds of amphiphilic copolymers such as diblock, triblock, or multiblock linear copolymers but also grafted or star copolymers. This large variety of amphiphilic macromolecules associated with different solvent conditions leads to numerous possibilities for structure formation and, as a consequence, to very different solution properties, ranging from viscous liquids to elastic gels. Also, the way copolymers adsorb at an interface may be influenced by their conformations in solution: the latter may either prevent copolymers from interacting with the interface due to structural solubility enhancement or be the precursors of the structures observed at the interface. Therefore, a first step to understand the possible structures of copolymers at an interface is to understand the possible conformations in solution. In the present study we will investigate the role of the size of the alternating hydrophilic and hydrophobic blocks in a multiblock copolymer on its self-assembly in dilute solutions. More precisely, we focus on the case of dilute solutions of linear copolymers made of hydrophilic (P for polar) and hydrophobic (H for hydrophobic) monomers arranged in a perfectly regular alternating multiblock pattern. Such macromolecules can model biopolymers such as hydrophobically substituted polysaccharides (e.g., cellulose derivatives[6]).

From an experimental point of view, a study by Kikuchi and Nose showed that amphiphilic graft copolymers made of poly(methyl metacrylate) (PMMA) and poly(styrene) (PS) are able to form unimolecular rodlike chains of micelles or unimolecular rodlike micelles depending on the quality of the solvent with respect to the backbone and the grafts.[7,8] Furthermore, studies on PNIPAM-g-PEO[9] and on copolymers with alternating segments of NIPAM and PS[10] reveal the existence of intramolecular core−shell micelles, although the structural effect of increasing chain length was not investigated. The intra- and intermolecular association of amphiphilic copolymers was addressed by Liu et al.,[11] emphasizing the importance of the distribution sequence of the hydrophobic segments on the self-assembly.

Similar questions were also addressed by theory and simulation. The case of random copolymers was extensively dealt with, and it was shown, either by simulation[12] or by theory,[13] that for a single copolymer several globular cores of H monomers surrounded by P monomers form. Vasilevskaya et al. used a different model to study the effect of the hydrophobic sequence on the collapse and structural polymorphism of amphiphilic copolymers in poor solvent for the H monomers. A variety of intramolecular conformations, such as strings of micelles or more elongated arrangements like cylindrical-shaped structures, were seen in simulations using either a P backbone with grafted attractive H side chains[14] or a copolymer consisting of a H backbone with two site amphiphilic/hydrophobic pairs[15] or alternating multiblock or protein-like copolymers made of a hydrophobic backbone with polar side monomers.[16] Also, the effect of chain flexibility on the collapsed conformations was addressed.[17] Finally, the H distribution along the chain (block length, random or regular) was shown to affect the temperature dependence and cooperativity of the coil−globule transition as well as the stability of the globule.[18] On the theoretical side, Halperin[19] predicted that a linear multiblock copolymer in the collapsed state may form a single intramolecular micelle or a

* To whom correspondence should be addressed. E-mail: virginie.hugouvieux@nantes.inra.fr.

10.1021/ma801337a CCC: $40.75
Published on Web 12/12/2008

string of molecular micelles depending on the length of the copolymer. Borisov and Zhulina studied the formation of and the transitions between different kinds of intramolecular structures (chains of micelles, tubes, lamellar structure) in the case of amphiphilic graft copolymers using a scaling theory.[20] A density functional approach was proposed for the case of amphiphilic molecules, where the monomer units consist of a hydrophobic group in the backbone and a hydrophilic side group.[21] Using this model the formation of several 'bead globules' per chain was predicted. Upon increasing the attraction between hydrophobic units, the latter merge and form either disklike or toruslike globules, depending on the chain stiffness. The collapse of multiblock copolymers into a unimolecular string of micelles was addressed by simulation using either a kinetic[22] or a structural point of view.[23] In a somewhat different context, pearl necklace-, cylinder-, and coil-type structures have been observed for polyelectrolytes as a result of the competition between electrostatic and hydrophobic interactions.[24] For short alternating multiblock copolymers the phase behavior has been shown to be influenced by the primary block lengths as well as the degree of polymerization of the blocks.[25]

In this work, our purpose is to gain insight into the generic behavior of amphiphilic linear multiblock copolymers in dilute solution. By computing experimentally accessible properties such as the radius of gyration or form factor, we want to characterize the different intramolecular structures obtained upon aggregation of the copolymers. At the same time, we want to identify the relevant parameters that control the different structures. Therefore, we focus on the conjugated effects of the hydrophobic substitution rate, the length of the hydrophilic and hydrophobic blocks, and the solvent quality for the hydrophobic monomers. Using lattice Monte Carlo simulations the structure of regular multiblock amphiphilic copolymers is determined as a function of the quality of the solvent for hydrophobic blocks through calculation of different radii of gyration, aggregation numbers, and form factors. The paper is organized as follows. In the next section, we introduce the model, describe the Monte Carlo method, and give details about the simulations performed. The results of the simulations are presented in section III. In section IV we discuss the different conformations and the corresponding form factors, and in section V we draw our conclusions.

II. Model, Method, and Simulation Details

We consider a dilute solution of copolymers, where intermolecular interactions can be neglected.

Model. Copolymers are modeled as chains of N_m connected monomers of two types, either hydrophobic (H) or hydrophilic (P). Since our interest is in dilute solutions, no intermolecular interactions are included, and therefore, we may consider the properties of a single copolymer. This copolymer is made of regularly alternating blocks of hydrophobic and hydrophilic monomers. Such copolymers are denoted as $(H_{B_H}P_{B_P})_n$, where B_H is the number of H monomers per hydrophobic block, B_P the number of P monomers per hydrophilic block, and n the number of $H_{B_H}P_{B_P}$ patterns in the polymer. A given multiblock copolymer thus consists of a total of $N_m = n(B_H + B_P)$ monomers, and its hydrophobic substitution rate, P_{sub}, is defined as

$$P_{sub} = \frac{nB_H}{N_m} = \frac{B_H}{B_H + B_P} \tag{1}$$

The solvent effect is simulated implicitly, and the interactions between the monomers and the solvent are accounted for indirectly. The repulsion between the hydrophobic monomers and the solvent is modeled by an effective short-range attractive interaction between the H monomers as the repulsion between hydrophobic monomers and the solvent favors association of the H monomers. One expects the relationship between the solvent quality and the interaction strength to be nonlinear but monotonic. In the model the interaction is restricted to nearest H neighbors, which corresponds to the range of repulsion between H monomers and solvent. This so-called hydrophobic interaction strongly depends on the quality of the solvent with respect to the H monomers. In practice, this interaction is taken into account through the effective energy E_i between neighboring H monomers: when $E_i = 0$, there is no interaction between H monomers and the quality of the solvent is equally good for both kinds of monomers; for increasing $|E_i|$, the solvent becomes increasingly poor for H monomers, which leads to formation of H clusters. Our model then takes into account different solvent qualities and various sizes and ratios of hydrophobic and hydrophilic blocks. The notion of good and poor solvent always refers to H monomers; P monomers are always in good solvent conditions. In summary, the interaction is always equal to zero between two hydrophilic monomers and between a hydrophilic and a hydrophobic monomer, while there is an attractive interaction of strength E_i between two hydrophobic monomers.

Monte Carlo Algorithm. The behavior of the multiblock copolymers is simulated using the algorithm of coarse-grained cell polymer dynamics developed by two of the authors.[26]

The basic idea of this model is to replace the complicated continuum dynamics of a polymer solution or melt by a truncated lattice version. Consider any continuum polymer system. To discretize this system we regularly divide space into compact cells. The centers of these cells form a regular lattice. The polymer conformation and its dynamics can then be uniquely discretized by placing all the monomers that lie in a given cell onto the corresponding lattice site. The cell size is a free parameter; for the present calculation we set it equal to two monomer volumes, i.e., each lattice site can be occupied by zero, one, or two monomers. After projection of the conformation onto the lattice the continuum dynamics becomes a nearest neighbor hopping dynamics. The bond lengths of the original model are also discretized to the values zero or one lattice spacing. This corresponds to a variation of the effective average bond length between one-half and one lattice spacing for a chain of doubly or singly occupied sites, respectively.

The original polymer model and the lattice model have the same properties on scales larger than a lattice spacing. Computationally a lattice model is much more efficient as the complicated continuum dynamics is replaced by a simple nearest neighbor hopping dynamics on the lattice. In order to reproduce statics and dynamics correctly, a lattice model must have three essential features of polymer structure and dynamics: the monomer connectivity along the chain, the excluded volume interaction, and the noncrossing of polymer strands. The connectivity requirement is assured by construction because neighboring monomers along the chain always sit on the same or nearest neighbor sites. The excluded volume restriction is respected automatically because each site can be occupied by at most two monomers. The condition that two polymer strands are not allowed to cross would require elaborate testing for the proposed discretization. To avoid this, we change the rules slightly: the double occupancy of a lattice site is restricted to monomers that are nearest neighbors along the same polymer chain (chemically bonded monomers). This is a minor change, which effectively corresponds to an increase of the range of the excluded volume interaction but allows one to guarantee the strict noncrossing of strands in a simple way.

The key difference between cell polymer dynamics and standard lattice models is that in our model a lattice site can be occupied by two monomers. This is also its main advantage:

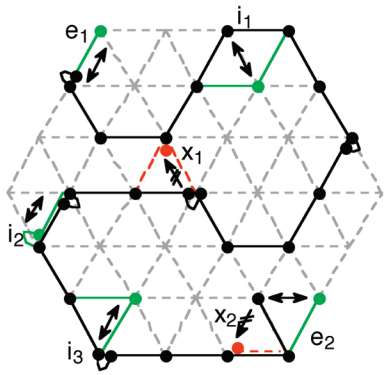

Figure 1. 2D representation of a polymer on the lattice and possible monomer moves. Black dots and bold lines represent an allowed conformation of the chain and its monomers. Green lines and dots are acceptable moves of end monomers (e_1, e_2) and internal monomers (i_1, i_2, i_3), respectively. Red lines and dots (x_1, x_2) show forbidden moves.

pure reptation along the polymer chain is explicitely possible even at the highest densities; monomers moving between a doubly occupied and an empty site naturally create local chain length fluctuations on the lattice; there are no locked up conformations and hence no ergodicity problems as for standard lattice models. The model is computationally efficient as it has, under athermal conditions, no adjustable parameters and only one move type. The unique space and time scales of this move correspond to the cell size and its characteristic relaxation time of the corresponding real polymer system. The model is designed in a way such that the cited three basic conditions of polymer dynamics are guaranteed by construction for every move. It can therefore be implemented as easily and efficiently as the simplest lattice models.

Let us now give the precise operational definition of cell polymer dynamics in three (two) dimensions as it is used here. (1) Conformation. (a) Each of the N_m monomers of a polymer is placed on a site of a periodic fcc (hexagonal) lattice. (b) Neighboring monomers along the chain (chemically bonded monomers) occupy either the same site or two nearest neighbor sites on the lattice. (c) No more than two monomers can occupy a lattice site. (d) Two monomers never occupy the same site if they belong to different polymers or if they belong to the same chain but are not neighbors along the chain. (2) Dynamics. (a) The dynamics consists of attempting to move a randomly chosen monomer to a randomly chosen nearest neighbor lattice site. (b) The move may be accepted if the new conformation is an allowed state according to the conformational rules above. The second conformational rule automatically guarantees the connectivity condition, the third rule the excluded volume, and the fourth rule the noncrossing of strands.

Figure 1 shows a two-dimensional (hexagonal) representation of the scheme. The choice of the fcc or hexagonal lattice is motivated by a greater number of nearest neighbors (12 and 6) and a wider and smoother range of bonding angles than a standard cubic (6) or square (4) lattice. A typical polymer conformation is shown along with various (allowed or forbidden) moves. Every allowed move naturally falls into one of two classes. (1) The following moves are reptation-like moves, i.e., the monomers move strictly along the chain: (a) an end monomer that moves from a doubly occupied site to an empty site or backward (e_1) and (b) an internal monomer that moves from a doubly occupied site to the singly occupied site of one of its two neighbors along the chain (i_2). In the first case the lattice chain length changes; in the second case it stays constant. (2) The following moves are Rouse-like moves, i.e., they displace the chain laterally: (a) an end monomer that moves from a singly occupied site to an empty site (e_2), (b) an internal monomer that moves from a singly occupied site to an empty site (i_1), and (c) an internal monomer that moves from a doubly occupied site to an empty site or backward (i_3). In the first two cases the lattice chain length stays constant; in the last case it changes.

Rouse-type moves dominate the dynamics for dilute solutions, whereas reptation moves dominate the dynamics at melt densities, just as expected for real polymers.[28] The shift from Rouse-dominated to reptation-dominated dynamics occurs naturally upon increasing the monomer density and without tuning of a parameter.

Examples of moves that are rejected because they would lead to forbidden conformations are also shown in Figure 1 (internal monomer x_1, end monomer x_2). Interactions are introduced by assigning every monomer to be H or P and adding an energy contribution $E_i < 0$ to the total energy for every pair of H monomers that either occupy the same site or occupy two nearest neighbor sites. When trying to move an interacting hydrophobic (H) monomer the move is only accepted if it is energetically favorable, according to the Metropolis sampling scheme.[27] The (dimensionless) energy difference ΔE of a conformation before and after a move is calculated, and the move is accepted if all other constraints are satisfied and if $\min(1, \exp(-\Delta E)) < \text{ran}$, where $0 \leq \text{ran} \leq 1$ is a uniformly distributed random number. Time is measured in Monte Carlo steps (MCS) which corresponds to $N_m N_p$ trial moves, where N_m is the total number of monomers per chain and N_p the number of chains in the system.

Simulation Details. For our simulations we use a $100 \times 100 \times 100$ lattice with periodic boundary conditions. To guarantee a dilute solution a single polymer ($N_p = 1$), whose size is far smaller than the lattice size, is simulated. Typical CPU simulation times for one set of parameter values vary from several hours to a few days on a standard PC.

Before presenting the data for the different copolymers we will show that the cell polymer dynamics model correctly describes the dynamics of a single noninteracting homopolymer.[26] A stringent criterion for the validity of any polymer model is the requirement that it correctly reproduces the time correlation functions $\langle \vec{X}_q(t) \cdot \vec{X}_q(0) \rangle$ of the exactly known eigenmodes of the Rouse model[27]

$$\vec{X}_q(t) = \frac{1}{N_m} \sum_{i=1}^{N_m} \vec{r}_i(t) \cos \frac{\pi q \left(i - \frac{1}{2}\right)}{N_m}, \text{ with } q = 0, 1, 2, \ldots N_m - 1$$

Rouse mode correlations for different q probe the dynamics on different length and time scales. The corresponding relaxation times τ_q depend (up to a constant) on q and N_m as $\tau_q = ((N_m)/(q))^2$.[28]

In Figure 2 the normalized correlations for different q values and chain lengths $N_m = 100$ and 400 for the Rouse model (neglecting excluded volume and strand crossing restrictions) are shown, plotted in scaled form against t/τ_q. The data collapse confirms that the model reproduces the dynamics correctly on all length scales, even for the shortest times. The simulated polymer conformation also has the expected Gaussian behavior. With excluded volume interactions the chains swell and their radius R scales with the number of monomers N_m with a fractal dimension $D = 1.69(3)$ in agreement with the Flory value.[28] This result is also confirmed by the form factor data presented below (see Figure 5). For such good solvent polymers the Rouse modes are no longer eigenmodes and the data collapse of Figure 2 fails.

When an attractive interaction is added between all monomers (homopolymer of H monomers) the polymer will undergo a collapse transition upon increasing the interaction strength. The good solvent regime is separated from the poor solvent regime

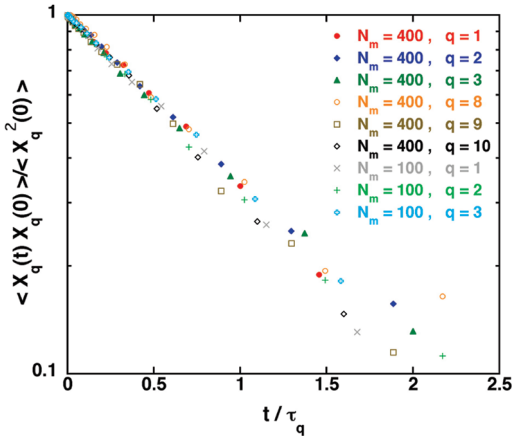

Figure 2. Time correlation of the Rouse modes for the cell polymer dynamics model. $\langle \bar{X}_q(t) \cdot \bar{X}_q(0) \rangle$, normalized by its value at $t = 0$ $\langle \bar{X}_q^2(0) \rangle$, is plotted logarithmically against t/τ_q for the three smallest q modes, $q = 1$, 2, and 3, for both $N_m = 100$ and 400 and three intermediate q modes, $q = 8$, 9, and 10, for $N_m = 400$. As predicted by the Rouse model, all data collapses onto a single straight line.

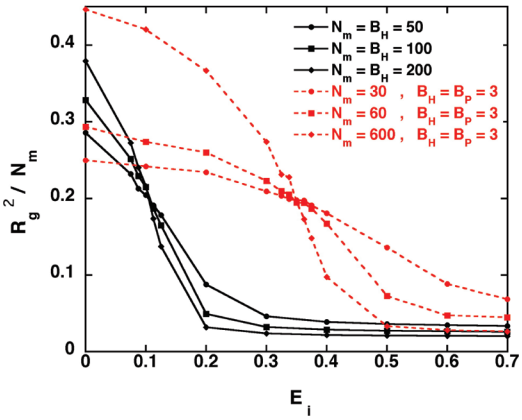

Figure 3. Ratio of mean square radius of gyration over chain length, R_g^2/N_m, versus dimensionless interaction energy E_i for different chain lengths N_m. The curves cross at the θ point, which separates the good solvent regime to the left from the bad solvent regime to the right of the θ point. The solid lines are data for homopolymers, where all monomers are hydrophobic (H) and interact; the dotted lines are for copolymers with $B_H = B_P = 3$ and only the hydrophobic H monomers interact.

by the θ point where the chain conformation is essentially Gaussian and the mean square radius of gyration R_g^2 scales linearly with N_m.

To verify that the model reproduces this change in conformation, we monitored the radius of gyration as a function of the energy for different chain lengths N_m. In Figure 3 the ratio R_g^2/N_m is plotted as a function of the dimensionless energy E_i for different chain lengths N_m. The crossing point of the different curves identifies the θ point. The figure clearly confirms the expected behavior, and the data qualitatively agrees with other polymer simulation results.[29] Note the rapid convergence of the θ point as determined from the crossing point of the curves for sucessive N_m. The numerical values of the energy E_i and ratio R_g^2/N_m at the θ point are of course model dependent. Along with the results for interacting homopolymers we also show the collapse of a $B_H = B_P = 3$ copolymer. The general behavior is the same, but the θ point of the copolymer is shifted to larger energy values because now only the H monomers interact with each other.

After having shown that the cell polymer dynamics model correctly reproduces polymer properties, both without and with

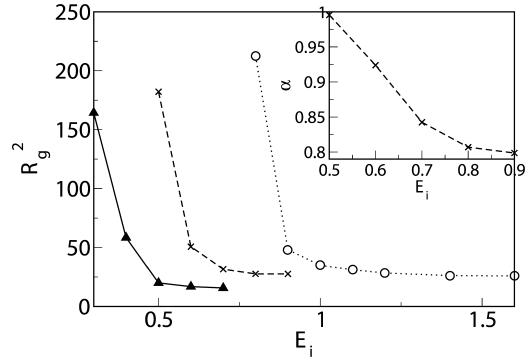

Figure 4. Mean squared radii of gyration as a function of E_i for $N_m = 600$ and $B_H = 3$. Dotted line: $P_{sub} = 0.1$. Dashed line: $P_{sub} = 0.3$. Full line: $P_{sub} = 0.5$. (Inset) Ratio $\alpha = R_{gH}^2/R_{gP}^2$ versus E_i for $P_{sub} = 0.3$.

Table 1. Simulated Systems[a]

P_{sub}	0.1	0.1	0.3	0.3	0.5	0.5	0.5	0.625	0.625
N_m	600	1200	600	900	600	1200	600	600	1200
B_H	3	3	3	3	3	3	2	5	5
B_P	27	27	7	7	3	3	2	3	3
energy	S,Q	S,Q	S,Q,R	S	S,Q,R	S	S	S	S

[a] Q stands for an energy quench, S for a step ramp, and R for a continuous ramp as detailed in the text.

interactions, we now discuss the structure formation of a copolymer. The systems were equilibrated during 10^8 MCS, and statistical averages were computed using configurations from the next 10^8 MCS. Equilibration was monitored using the autocorrelation function of the end-to-end vector as a relaxation criterion. For each set of parameters, eight independent runs were performed and statistical averages computed using 100 equally spaced configurations in each run.

In order to optimize the equilibration of the initial configurations the simulations were performed for increasingly larger values of E_i: starting from a given interaction energy E_i, a set of independent samples is equilibrated and a production run is performed. In the next step, the equilibrated configurations at E_i are used as starting configurations for the equilibration and production runs at $E_i + \delta E_i$. This scheme is iterated from the E_i of a good solvent to E_i corresponding to a poor solvent. To verify that equilibrium has actually been reached, the equilibrium configurations obtained from this method have been compared with simulations obtained by either quenching to a poor solvent or cooling very slowly (continuous energy ramp) from good to poor solvent. The results are the same except for some very deep quenches, where slow cooling produces somewhat more ordered structures.

In the limit of long chains with a large number of blocks, the parameters of interest are the hydrophobic substitution rate P_{sub} and the interaction energy E_i between H monomers. We performed simulations for hydrophobic substitution rates ranging from 0.1 to 0.625 and for energies in the range $|E_i| \in [0.0, 1.3]$. Details of the simulated copolymers are given in Table 1.

The lattice spacing is taken to be the unit of length, and energy is measured in kT and enters in the simulations in its dimensionless form E_i.

III. Simulation Results

Simulations give access to different kinds of information. Direct visual inspection of the conformations and their evolution with time gives a first insight into the structure and dynamics of the mesostructures as a function of the parameters. A more quantitative analysis can be made from calculating structural properties of the simulated configurations: In this work we focus on several radii of gyration, the size of H clusters, and different form factors. Both the radii of gyration and the form factors

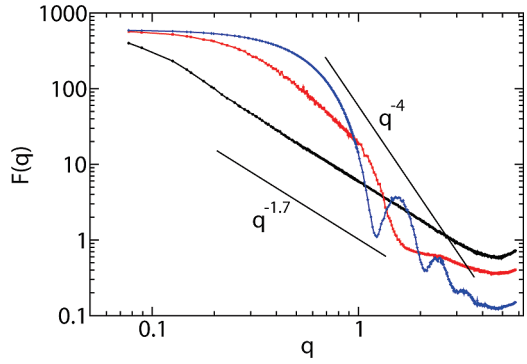

Figure 5. Total form factors for different values of P_{sub} with $N_m = 600$ and $B_H = 3$. Good solvent conditions: $E_i = 0.0$ (black line). Poor solvent conditions: $P_{sub} = 0.3$, $E_i = 0.9$ (red line); $P_{sub} = 1$, $E_i = 0.4$ (blue line).

are also available from experiments. Confronting visual inspection and statistical properties allows one to identify the signature of each conformation that is expected in an experimental measurement (e.g., scattering experiment).[30]

III.A. From Good Solvent to Poor Solvent. We first focus on the effect of the interaction energy E_i between H monomers on the overall size of the chain. The copolymer is characterized by its radius of gyration R_g, computed as

$$R_g^2 = \frac{1}{N_m}\left\langle \sum_{i=1}^{N_m} (\vec{r}_i - \vec{r}_{cm})^2 \right\rangle \quad (2)$$

where $\vec{r}_i$ is the position of monomer i and $\vec{r}_{cm}$ is the position of the center of mass of the polymer at a given time, and $\langle . \rangle$ denotes an average over all configurations.

Figure 4 shows the evolution of the average value of the squared radius of gyration of the copolymer with the interaction energy E_i for chain length ($N_m = 600$) and H block size ($B_H = 3$) for three values of P_{sub} ($P_{sub} = 0.1$, 0.3, and 0.5). We observe the expected behavior from a swollen state with large R_g^2 at low values of E_i (good solvent) to a more compact state with high solvent selectivity (poor solvent for H monomers). Decreasing the length of the noninteracting P blocks while keeping the H block length fixed (i.e., increasing P_{sub}) shifts the collapsed region to weaker energies. The same effect is observed when increasing simultaneously the lengths of interacting and noninteracting blocks while keeping P_{sub} fixed (not shown here), in agreement with previous findings.[18]

Similar quantities can also be computed for H (and P) monomers separately by replacing N_m by the total number of H (and P) monomers in the chain. The ratio α of the squared hydrophobic and hydrophilic radii of gyration is shown as the inset in Figure 4. Note that R_{gH} and R_{gP} give insight into the positions of all the H and P monomers relative to the center of mass of the chain. For weak interactions, the extent of hydrophobic and hydrophilic parts of the copolymer are indistinguishable since the solvent is equally good for both kinds of monomers. With increasing E_i hydrophobic monomers tend to be buried in the collapsed coil, while the outer shell of the polymer conformation is mainly occupied by hydrophilic monomers, as shown by the decreasing ratio $\alpha = R_{gH}^2/R_{gP}^2$. The data clearly confirms that collapse of the copolymers is not homogeneous. This aspect can be further investigated by calculating the form factors of the copolymers.

Form factors are a unique tool for determining the multiscale structure of polymers and are experimentally accessible using either neutron or X-ray scattering. In simulations the corresponding form factor can be computed using the following equation[31]

$$F(q) = \frac{1}{N_m}\left\langle \sum_{j,k=1}^{N_m} \exp[i\vec{q}\cdot(\vec{r}_j - \vec{r}_k)] \right\rangle \quad (3)$$

Since the system is isotropic, the form factor can be averaged over all $\vec{q}$ vectors of equal length using the scheme described in ref 32. The average $\langle . \rangle$ is also performed over all configurations. We limit the analysis of the form factor at large q to $q < 2\pi/a$, where a is the lattice spacing, as for $q \gtrsim 2\pi/a$ the scattering intensity is dominated by lattice effects. We assume here that the scattering lengths of both kinds of monomers are equal. Figure 5 shows the form factors of the chains under different solvent conditions and for two values of P_{sub}. At $E_i = 0$ the solvent is equally good for H and P monomers and the copolymer shows a fractal dimension of 1.7 in the intermediate q range, typical of homopolymers in good solvent with $F(q) \propto q^{-1.7}$. For interaction energies typical of poor solvents (as determined from the energy dependence of R_g, see Figure 4), several features can be noticed. The low q region of $F(q)$, for $qR_g \ll 1$, gives access to the overall size of the copolymer using the Guinier approximation.[33] Figure 5 is in agreement with the observations of the evolution of R_g with a compaction of the coil as E_i increases for fixed P_{sub}. In a poor solvent the plateau is reached at larger q values (smaller values of R_g). In the intermediate q range, for $qR_g \geq 1$, one probes the internal structure of the polymer. In particular, $F(q) \propto q^{-4}$ characterizes a compact spherical structure. A homopolymer ($P_{sub} = 1$) under poor solvent conditions is expected to collapse into such a compact spherical structure. The data in Figure 5 nicely reproduces this behavior, all the way up to $q \approx \pi$. For larger q values lattice effects are expected to appear and dominate $F(q)$. This is hinted by the upturn of $F(q)$ at 2π in all cases studied. For P_{sub} values different from $P_{sub} = 1$ (red line in Figure 5) the behavior is different and correlations appear at intermediate q values, which become more pronounced with increasing E_i at fixed P_{sub} (not shown).

Note that the form factors in poor solvent conditions are not shown for the same interaction energies in order to account for the variation with substitution rate of the interaction energy needed for the copolymer to collapse.

The presence of correlation lengths in $F(q)$, as shown by the shoulder at $q \approx 1$, suggests the existence of mesostructures with characteristic lengths smaller than the overall chain size R_g in poor solvent. This observation is likely to be related to the existence of dense clusters of H monomers, as indicated by the decreasing ratios of hydrophobic to hydrophilic radii of gyration (Figure 4). To check this hypothesis we identified hydrophobic clusters in the simulated conformations. For our purpose a cluster is defined as a set of interacting H blocks. Two blocks are said to interact if any two monomers of these blocks are nearest neighbors. This property is transitive; if block A interacts with block B and block B with block C then all three belong to the same cluster. Considering clusters of blocks or of their monomers is equivalent, of course. The aggregation number N_C of a cluster is defined as the number of H blocks belonging to this cluster.

From the cluster size distributions data for different values of P_{sub} and E_i and for sufficiently long chains ($N_m = 600$) we distinguish two main types of behavior, shown in Figures 6 and 7. Figure 6 shows the typical aggregation behavior for low substitution rates ($P_{sub} \leq 0.3$), while Figure 7 is typical of higher P_{sub} values. Not surprisingly, in both cases a decrease of the probability of finding isolated H blocks with increasing interaction energy E_i is observed. Direct visual inspection of time sequences shows that the exchange of individual H blocks between clusters also becomes more and more rare. For low P_{sub} in a poor solvent a distribution of cluster sizes appears around a well-defined average value N_c. With increasing energy

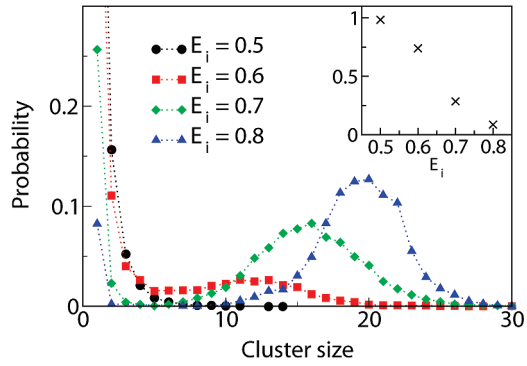

Figure 6. Probability distribution (number probability) of cluster sizes and their evolution with interaction energy from $E_i = 0.5$ (good solvent) to 0.8 (poor solvent). The copolymer is defined as $(H_{B_H}P_{B_P})_{60}$ with $N_m = 600$, $B_H = 3$, $B_P = 7$, and $P_{sub} = 0.3$. The cluster size is expressed in numbers of hydrophobic blocks. The probability is negligible beyond $N_c \geq 30$. The inset shows the total fraction of small clusters ($N_c < 5$) as a function of E_i.

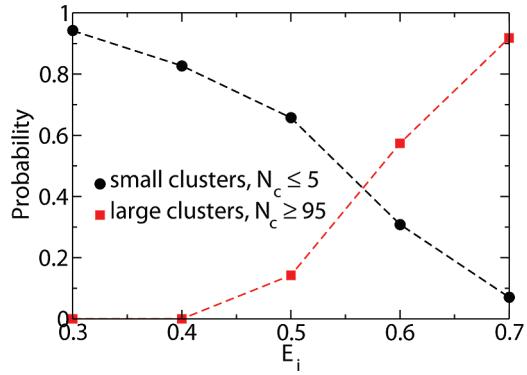

Figure 7. Probability of forming small ($N_C \leq 5$) and large ($N_C \geq 95$) clusters as a function of E_i. The polymer number of H blocks is 100. $P_{sub} = 0.5$, $N_m = 600$, $B_H = 3$, $B_P = 3$. For $E_i = 0.4$ the solvent is good, and for $E_i = 0.7$ the solvent is of very poor quality for the H monomers.

E_i the peak of the distribution becomes sharper and shifts to higher values. This is particularly clear for $P_{sub} = 0.3$ (see Figure 6). For $E_i = 0.8$ there are $\langle N_c \rangle \approx 20$ blocks in a cluster, which corresponds to an average of three H clusters per chain. For $P_{sub} = 0.1$ the same general picture is observed but with the interaction energies shifted to higher values. For $N_m = 600$ and $B_H = 3$ there are only 20 H blocks in the copolymer and a single cluster with $\langle N_c \rangle \approx 20$. Therefore, simulations with $N_m = 1200$ were performed: an average of two clusters is observed which supports the expectation that the number of clusters is growing with the chain length and the size distribution (aggregation number) is independent of chain length. For $P_{sub} = 0.1$ and $E_i > 1.0$ the data show signs that the system is not fully equilibrated on the time scales considered.

For large values of P_{sub}, $P_{sub} = 0.5$, the cluster size distribution is qualitatively different from small P_{sub}. Up to $E_i = 0.4$ no well-defined cluster is present; beyond $E_i = 0.5$ almost all H blocks collapse into a single cluster, as evidenced in Figure 7.

The radius of gyration is a simple test for distinguishing good and poor solvent behavior. The form factor proves to be a more sensitive tool as it shows a transition from a homopolymer behavior in a good solvent to a complex structure with mesoscale correlation lengths in a poor solvent. In a poor solvent the cluster size distribution distinguishes between a well-defined cluster size that depends on the solvent quality for small P_{sub} and a single large cluster that depends little on solvent quality for large P_{sub}. For a full understanding of these observations

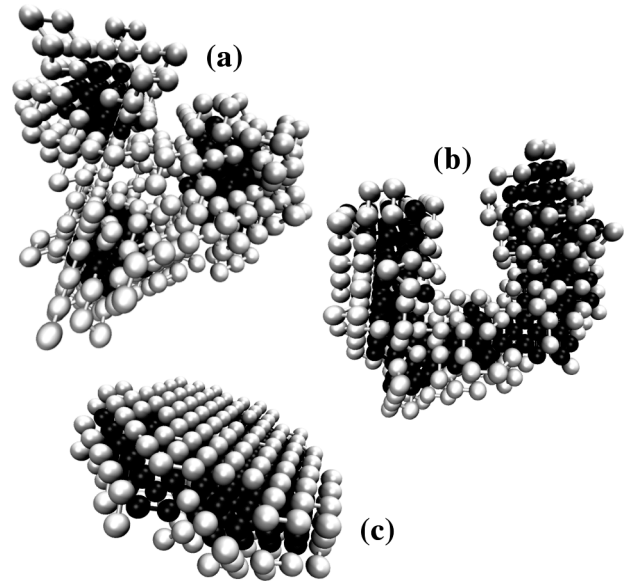

Figure 8. Typical configurations for different substitution rates: (a) $P_{sub} = 0.3$, chain of micelles; (b) $P_{sub} = 0.5$ with $B_H = 3$, tubular structure; (c) $P_{sub} = 0.5$ with $B_H = 2$, layered structure. H monomers are depicted in black and P monomers in light gray.

the detailed intramolecular structures in poor solvent need to be analyzed.

III.B. Intramolecular Structures in Poor Solvent. The first insight into the intramolecular structures in poor solvent can be obtained from the direct visualization of copolymer conformations. We notice several well-defined features, as shown in Figure 8.

For $P_{sub} \leq 0.3$ we observe the formation of intramolecular chains of micelles (a single intramolecular micelle for short chains). The H blocks aggregate into clusters (see Figure 6) which are surrounded by P blocks (see Figure 8a). These clusters typically are spherical or ellipsoidal, and they are linked to each other by one or several P blocks. The number of such intramolecular clusters increases linearly with N_m.

For $P_{sub} \geq 0.5$, when decreasing the solvent quality, the copolymer undergoes a transition from a swollen chain to a chain containing H aggregates and then to a single cluster containing all H blocks, no matter how long the copolymer. The evolution of N_c shows this quantitatively (see Figure 7). There are two different types of structures observed in the very poor solvent single cluster regime with $P_{sub} = 0.5$. For $B_H = B_P = 3$ upon increasing the energy there first appears a tubular-shaped single cluster (the tube may be open, torus-like, or with its ends folded back anywhere onto the tube) and for stronger energies a layered structure with a hydrophobic inner layer (crystalline, possibly distorted and with defects), see Figure 8. The transition from tubular to layered structure with increasing E_i proceeds via formation of a chain of growing pieces of the layered structure. The transition from the tubular to the layered structure is most clearly seen in simulations using a slowly increasing energy ramp. Formation of a tubular and then a layered structure upon increasing the energy is also observed for $B_H = 5$ and $B_P = 3$. On the other hand, for $B_H = B_P = 2$ there is no tubular structure and the layered cluster is formed directly with poorer solvent quality. In this case the layered structure is much more regular and the surfaces are much smoother than the previous ones.

A more detailed analysis of the intramolecular structures can be obtained from the partial structure factors $F_H(q)$, $F_{cluster}(q)$, and $F_P(q)$, see Figures 9, 10 and 11. $F_H(q)$ ($F_P(q)$) gives information about the correlations between all H (all P)

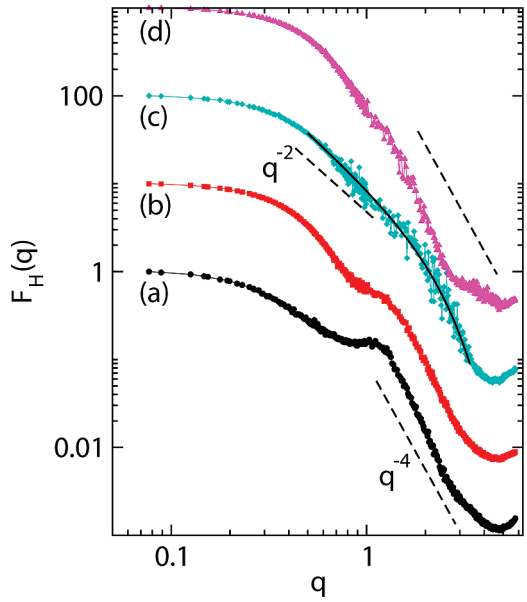

Figure 9. Partial form factor of hydrophobic monomers under poor solvent conditions: (a) $P_{sub} = 0.3$, $N_m = 600$, $B_H = 3$, $B_P = 7$, $E_i = 0.9$ (chain of micelles); (b) $P_{sub} = 0.5$, $N_m = 600$, $B_H = 3$, $B_P = 3$, $E_i = 0.7$ (tubular structure); (c) $P_{sub} = 0.5$, $N_m = 600$, $B_H = 2$, $B_P = 2$, $E_i = 0.7$ (layered structure); (d) $P_{sub} = 0.625$, $N_m = 600$, $B_H = 5$, $B_P = 3$, $E_i = 0.8$ (layered structure with rough surfaces and defects). Solid line: analytical form factor of a 2d platelet. Note that the curves are normalized by N_H and shifted vertically by 1 order of magnitude for clarity.

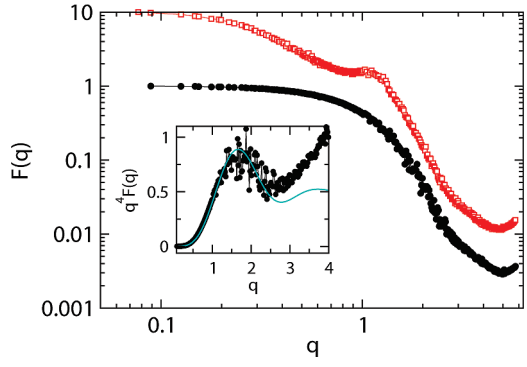

Figure 10. Form factor of H monomer (red squares) and H clusters (black circles) for $P_{sub} = 0.3$, $N_m = 600$, $B_H = 3$, $B_P = 7$, $E_i = 0.9$. Note that the form factors are normalized and shifted. (Inset) Porod representation of $F_{cluster}(q)$ (black circles, same set of parameters). Solid line: analytical form factor of a sphere of radius $R_s = 1.8$ and polydispersity $dR_s = 0.3$.

monomers, whereas $F_{cluster}(q)$ correlates H monomers within the same cluster and can be used for characterizing the shapes and sizes of the H clusters (see section III.A). $F_H(q)$, $F_P(q)$, and $F_{cluster}(q)$ are defined by eq 3, where the summation is restricted to the H monomers, P monomers, and H monomers belonging to a given cluster, respectively. Note that we restrict our study to $F_H(q)$ and $F_P(q)$, bearing in mind that the cross-correlations $F_{HP}(q)$ will also have an impact on the total form factor $F(q)$.[31] Let us first focus on the properties of $F_H(q)$ (Figure 9) and $F_{cluster}(q)$ (Figure 10). The cluster form factors for $P_{sub} > 0.3$ are not shown since $F_H(q) \approx F_{cluster}(q)$ as most H blocks belong to a single cluster.

For small q values $F_H(q)$ reaches a plateau, which corresponds to the Guinier regime where $qR_g \ll 1$. For intermediate q values $F_H(q)$ tends to behave as q^{-4}, which stands for a compact object with a sharp interface (well-defined density drop). This feature is independent of P_{sub}, and in this range of q values $F_H(q)$ and

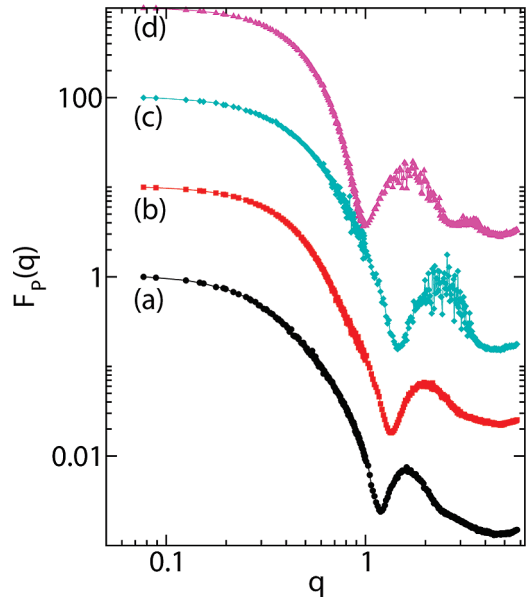

Figure 11. Partial form factors of hydrophilic monomers in poor solvent conditions: (a) $P_{sub} = 0.3$, $N_m = 600$, $B_H = 3$, $B_P = 7$, $E_i = 0.9$ (chain of micelles); (b) $P_{sub} = 0.5$, $N_m = 600$, $B_H = 3$, $B_P = 3$, $E_i = 0.7$ (tubular shape); (c) $P_{sub} = 0.5$, $N_m = 600$, $B_H = 2$, $B_P = 2$, $E_i = 0.7$ (layered structure); (d) $P_{sub} = 0.625$, $N_m = 600$, $B_H = 5$, $B_P = 3$, $E_i = 0.8$ (layered structure with rough surfaces). Note that curves are normalized by N_H and shifted vertically for clarity.

$F_{cluster}(q)$ can be superimposed (adjusting the scales appropriately). For $P_{sub} = 0.3$, $F_{cluster}(q)$ can be fitted to the analytical form factor of a polydisperse sphere of radius $R_s = 1.85$ (see Figure 10). For lower q values the behaviors of $F_H(q)$ and $F_{cluster}(q)$ depart from each other for $P_{sub} = 0.3$: $F_H(q)$ shows a well-defined correlation distance at $q_c \approx 1.2$ ($\approx$5.2 lattice units in real space), which becomes more pronounced for longer chains and disappears for short chains (single intramolecular micelle). Therefore, this correlation peak reflects the average distance between H clusters: It is absent in the case of a single cluster and increases when the number of clusters and hence the number of intercluster distances increases. For $P_{sub} = 0.5$ and $B_H = 3$ (see Figure 9b) we observe an inflection point around $q \approx 1.3$, which turns into a short plateau for longer chains ($N_m = 1200$, not shown here). As explained above (and detailed in section III.A) there is a single cluster of H monomers, and this inflection point might correspond to the mean distance between monomers on opposite sides of closed tubular conformations, predominant in this case. This hypothesis is supported by the fact that the intensity at which the inflection occurs increases with increasing E_i, when the structure becomes better defined. For $P_{sub} = 0.5$ and $B_H = 2$ $F_H(q)$ becomes quite different with the onset of a q^{-2} behavior at intermediate q values, which is typical of two-dimensional structures. For higher q the structure is compact with a q^{-4} slope. The H blocks form a compact two-dimensional structure. The same kind of behavior is observed for $P_{sub} = 0.625$ with $B_H = 5$ and $B_P = 3$; however, the onset of the q^{-2} behavior is not observed for two reasons. For the same value of N_m, the layer is thicker and its surface area smaller than for $B_H = 2$, which reduces the range of the q^{-2} behavior. At the same time, the surface is much rougher and shows more defects for $P_{sub} = 0.625$, which leads to an effective surface fractal dimension $d_g \geq 2$.

If we now move on to the contribution from the P monomers (Figure 11), the salient feature of $F_P(q)$ is the peak at a q_P value between 1 and 2, depending on P_{sub}: It shifts to larger q values (smaller distances) and becomes more pronounced when P_{sub} increases from 0.3 to 0.5, indicating a stronger correlation and a more regular arrangement of the P monomers with increasing

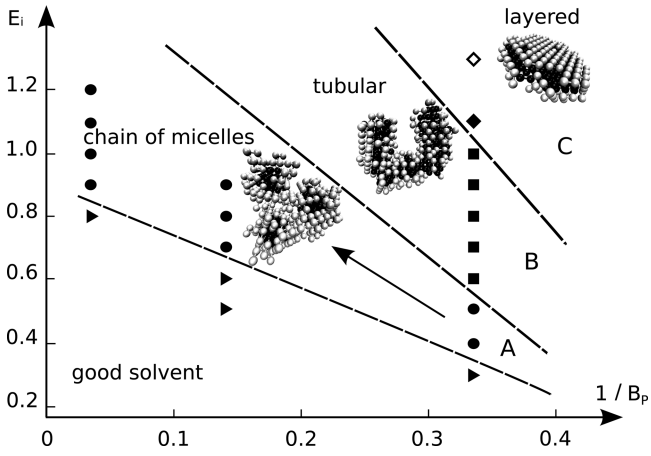

Figure 12. Phase diagram of the intramolecular structures of multiblock copolymers as a function of E_i and $1/B_P$ for $B_H = 3$. Symbols denote simulated systems with equilibration at constant energy (solid symbols) or an energy ramp (open symbol). Copolymers in good solvent are denoted as triangles, pearl neacklaces of micelles as dots, tubular structures as squares, and layered structures as diamonds. Dashed lines indicate the boundaries between the phases corresponding to the different structures. Snapshots show typical conformations observed in the simulations. The arrow points in the direction where a simultaneous increase of E_i and B_P maintains the energy−entropy balance necessary for stabilizing a given structure.

P_{sub}. For $P_{sub} = 0.625$, the main peak shifts to smaller q values and a secondary peak appears. The most straightforward case to interpret is the two-dimensional platelet of H blocks, as found for $P_{sub} = 0.5$ with $B_H = 2$ and $P_{sub} = 0.625$ with $B_H = 5$. Due to connectivity constraints, the P blocks must coat the surfaces of the H platelet and consequently $F_P(q)$ has a scattering function similar to that of stacked lamellae. For such structures, peaks are expected at $q_c = (2n\pi)/(d)$ with widths $\Delta q = (2\pi)/(nd)$, where d is the spacing between two consecutive lamellae.[34] For $P_{sub} = 0.5$ with $B_H = 2$, we obtain a value $d \approx 2.6$ (from both the position and the width of the peak), and for $P_{sub} = 0.625$ with $B_H = 5$, $d \approx 3.8$ (independently and consistently determined from the positions and the widths of the two peaks). These values are slightly larger than the thickness of the H layer and correlate with the distance between the P layers.

For the other two cases the situation is quite different. For $P_{sub} = 0.5$ ($B_H = B_P = 3$) the peak is at $q_P \approx 1.95$, and for $P_{sub} = 0.3$ ($B_H = 3$, $B_P = 7$) it is at $q_P \approx 1.6$. The corresponding distances $d_p = (2\pi)/(q_P)$ are $d \approx 3.2$ and 3.9, respectively. They can be associated with the tube diameter and sphere diameter of the hole due to the presence of the H core. In particular, for $P_{sub} = 0.3$, $d \approx 3.9$ agrees well with the size of the H core determined by fitting $F_H(q)$ to the analytical form factor of a sphere (see Figure 10).

IV. Discussion

Comparing the statistical properties extracted from the simulations with direct visualization of the intramolecular structures we are able to give an accurate description of the conformations of single multiblock copolymers as a function of solvent quality in terms of the form factors.

For weak interaction energies the copolymer trivially has the properties of a swollen coil, as shown by $F(q) \propto q^{-1.7}$. The transition from good to poor solvent is accompanied by the formation of fluctuating aggregates due to the attractive interaction between H monomers. With increasing values of E_i, after individual collapse of the hydrophobic blocks different intramolecular structures develop. This is shown in the phase diagram, Figure 12, as a function of energy E_i and hydrophilic block length B_P. With increasingly poorer solvent the qualitatively different conformations encountered are, in order, chains of micelles (see region A in Figure 12), tubular structures (region B), and layered structures (region C). The diagram corresponds to a given value of B_H ($B_H = 3$ in Figure 12), but it is similar for other values of B_H. The parameters E_i and B_P (or $1/B_P$ in the diagram) are used because the observed structures result from a balance between energy and entropy: E_i governs the energy contribution of the interacting H monomers, while B_P is a measure for the configurational entropy of the P blocks. Different values of B_H change the size of the elementary H cores but do not change the principle of the energy−entropy balance responsible for the different structures.

In region A of Figure 12 intramolecular pearl necklaces of core−shell micelles are formed with a well-defined core size of the micelles. The size of the pearls is stabilized by the P shells: Increasing the size of the H clusters, for a given E_i and B_P, would lead to an important entropy penalty due to the crowding of the P shell; decreasing the size of the H cores would induce an energy loss that is not compensated by a sufficient entropy gain. For each energy E_i and for every pair of H and P block lengths there is a core size that balances the energetic and entropic forces. As a consequence, a simultaneous increase of E_i and B_P in region A (see the arrow) keeps the topology of the structure unchanged: strengthening E_i tends to increase the size of the H cores; increasing the length of the P blocks reinforces the protective corona of the micelles and tends to decrease the core size. The data points in Figure 12 as well as the simulations for other values of B_H fully confirm this mechanism of balancing entropy and energy. In addition, simulations with longer chains confirm that the chain length has no influence on the micelle structure.

Moving now to region B, formation of tubular-shaped structures with a hydrophobic core is observed. Such a tubular core is energetically more favorable than the spherical cores of region A, but it has less surface area available for the hydrophobic corona. With respect to region A, region B corresponds to either copolymers with shorter P blocks (larger $1/B_P$), thus reducing the entropic contribution, or larger energies E_i or both. Again, the length of the copolymer has no influence on the structure of the tube. The energy E_i does have an effect on the detailed shape of the tube: for smaller values the core of the tube and its corona have a spherical cross-section, whereas for larger energies small parts of the tube locally begin to form pieces of layered domains as a precursor to the third morphology.

In region C one observes two-dimensional disklike layered structures with an inner H layer and two outer P layers. With respect to B this morphology requires a further increase of the energy E_i and/or a decrease of the length of the hydrophilic blocks B_H. As the equilibration at such high energies takes very long, these structures are simulated best using a ramp of slowly increasing E_i. Besides the data point for $B_H = 3$ shown in Figure 12 similar structures were obtained for $E_i \approx 0.7$ for $B_H = B_P = 2$ and for $B_H = 5$, $B_P = 3$. The most perfect crystalline structures were obtained for $B_H = B_P = 2$, whereas for $B_H = 5$ and $B_P = 3$ the resulting crystal is less perfect and with a rougher surface. This difference can be explained by the very short H and P blocks for $B_H = B_P = 2$, which impose a strong restriction on the hydrophobic monomers during formation of the layer.

Simulations with other values of B_H confirm the morphologies and their dependence on the parameters. The transitions chain of aggregates → tubular shape → disklike layered structure with increasing E_i is not only observed for $B_H = B_P = 3$ but also for $B_H = 3$ and $B_P = 5$ with energies $E_i = 0.5$ and 0.7, respectively. Purely energetic considerations suggest that for sufficiently large values of E_i the layered structure is always favored, no matter how long the B_P blocks. This is because inclusion of P beads

in a homogeneously collapsed phase would be energetically too costly at such high interaction energies. The different morphologies and their order in the phase diagram can be understood as a result of the competition between entropy and energy: starting from the origin, the same morphological changes are expected from an entropy decrease (horizontally) and an energy increase (vertically).

The different morphologies found in our simulations can be compared with the theoretical work based on scaling arguments by Borisov and Zhulina[20] on amphiphilic graft copolymers with hydrophobic backbone: Even though a graft polymer differs from our copolymer, they predict formation of analogous structures (necklace of starlike or crew-cut micelles, cylindrical wormlike micelle, and lamellar structure) depending on the degree of branching of the copolymer and solvent quality. Despite the different connectivity constraints for the two polymers, the expected conformations are similar. In the case of a graft copolymer, the collapse of the spacer is limited by the repulsion between side chains, while in the case of a multiblock copolymer, the entropic penalty which limits aggregation of H blocks comes from the P blocks that surround the corresponding H cluster. Sparse grafting may be compared to a high substitution rate, and dense grafting corresponds to multiblock copolymers with few associating monomers.

On the experimental side, the study of Zhang et al.[10] corresponds to $1/B_P \approx 0.015$ with ~230 H blocks per chain. As reported in ref 10 a single core−shell micelle is observed experimentally, which according to our understanding is the limiting case of a pearl necklace of micelles. This suggests that experiments performed with longer chains would have led to the formation of a chain of several micelles. The studies by Wu et al.[9] and Kikuchi and Nose[7,8] were performed on graft copolymers. Wu and Qiu[9] observed a large decrease of R_g and R_g/R_h upon increasing temperature and interpreted this as a transition from a coil to a core−shell structure. However, they did not characterize the shape of the collapsed state. On the other hand, Kikuchi and Nose revealed two kinds of behavior: when the grafts are in poor solvent (for $1/B_P$ between 0.02 and 0.08) the copolymers tend to form intramolecular rodlike chains of micelles, while for a poor solvent for the backbone (corresponding to large values of $1/B_P$) formation of unimolecular rodlike micelles is suggested. Although connectivity and flexibility constraints are quite different in linear and graft copolymers, the structures observed by Kikuchi and Nose are in qualitative agreement with the behavior observed in the simulations. A difference is the rodlike character of the intramolecular structures proposed by Kikuchi and Nose, not observed in our simulations. It may be related to the difference in connectivity constraints between graft and linear copolymers.

V. Conclusion

Lattice Monte Carlo simulations of regular amphiphilic multiblock copolymers in a dilute solution reveal the formation of different kinds of intramolecular structures depending on the interaction strength between the hydrophobic monomers and the length of the hydrophilic blocks. For any given value of the parameters the stable structure, made of a hydrophobic core surrounded by a protective hydrophilic layer, is determined by the balance between energetic (hydrophobic) and entropic (hydrophilic) contributions. Quantitative properties, such as the aggregation number or various radii of gyration and form factors, together with direct visualization of the configurations provide a coherent description of the morphologies and the transitions between them. A detailed analysis of the form factor allows for an experimentally accessible differentiation between the various conformations. These results show that modeling and simulation are helpful tools to design multiblock copolymers with controlled properties.

Acknowledgment. The IDRIS (Orsay, France), CINES (Montpellier, France), and CCIPL (Nantes, France) computer centers are acknowledged for the provision of computer time.

References and Notes

(1) Alexandridis, P.; Lindman, B. *Amphiphilic block copolymers: Self-assembly and applications*; Elsevier: Amsterdam, 2000.
(2) Riess, G. *Prog. Polym. Sci.* **2003**, *28*, 1107–1170.
(3) Bhatia, S. R.; Mourchid, A.; Joanicot, M. *Curr. Opin. Colloid Interface Sci.* **2001**, *6*, 471–478.
(4) Kataoka, K.; Harada, A.; Nagasaki, Y. *Adv. Drug Delivery Rev.* **2001**, *47*, 113–131.
(5) Fatimi, A.; Tassin, J.-F.; Quillard, S.; Axelos, M. A. V.; Weiss, P. *Biomaterials* **2008**, *29*, 533–543.
(6) Hirrien, M.; Chevillard, C.; Desbrieres, J.; Axelos, M. A. V.; Rinaudo, M. *Polymer* **1998**, *39*, 6251–6259.
(7) Kikuchi, A.; Nose, T. *Macromolecules* **1996**, *29*, 6770–6777.
(8) Kikuchi, A.; Nose, T. *Polymer* **1996**, *37*, 5889–5896.
(9) Wu, C.; Qiu, X. P. *Phys. Rev. Lett.* **1998**, *80*, 620–622.
(10) Zhang, G. Z.; Winnik, F. M.; Wu, C. *Phys. Rev. Lett.* **2003**, *90*, 035506.
(11) Liu, R.; Pallier, A.; Brestaz, M.; Pantoustier, N.; Tribet, C. *Macromolecules* **2007**, *40*, 4276–4286.
(12) Kuznetsov, Y. A.; Timoshenko, E. G.; Dawson, K. A. *J. Chem. Phys.* **1995**, *103*, 4807–4818.
(13) Ganazzoli, F. *J. Chem. Phys.* **2000**, *112*, 1547–1553.
(14) Vasilevskaya, V. V.; Klochkov, A. A.; Khalatur, P. G.; Khokhlov, A. R.; ten Brinke, G. *Macromol. Theory Simul.* **2001**, *10*, 389–394.
(15) Vasilevskaya, V.; Khalatur, P.; Khokhlov, A. *Macromolecules* **2003**, *36*, 10103–10111.
(16) Vasilevskaya, V. V.; Klochkov, A. A.; Lazutin, A. A.; Khalatur, P. G.; Khokhlov, A. R. *Macromolecules* **2004**, *37*, 5444–5460.
(17) Vasilevskaya, V. V.; Markov, V. A.; Khalatur, P. G.; Khokhlov, A. R. *J. Chem. Phys.* **2006**, *124*, 144914.
(18) van den Oever, J. M. P.; Leermakers, F. A. M.; Fleer, G. J.; Ivanov, V. A.; Shusharina, N. P.; Khokhlov, A. R.; Khalatur, P. G. *Phys. Rev. E: Stat., Nonlinear, Soft Matter Phys.* **2002**, *65*, 041708.
(19) Halperin, A. *Macromolecules* **1991**, *24*, 1418–1419.
(20) Borisov, O.; Zhulina, E. *Macromolecules* **2005**, *38*, 2506–2514.
(21) Ushakova, A. S.; Govorun, E. N.; Khokhlov, A. R. *J. Phys.: Condens. Matter* **2006**, *18*, 915–930.
(22) Cooke, I. R.; Williams, D. R. M. *Macromolecules* **2003**, *36*, 2149–2157.
(23) Koga, T. *Eur. Phys. J. E* **2005**, *17*, 381–388.
(24) Chodanowski, P.; Stoll, S. *J. Chem. Phys.* **1999**, *111*, 6069–6081.
(25) Gindy, M. E.; Prud'homme, R. K.; Panagiotopoulos, A. Z. *J. Chem. Phys.* **2008**, *128*, 164906.
(26) Kolb, M.; Axelos, M. A. V. Rouse and reptation dynamics: a polymer lattice model. *XV Conference of the European Colloid and Interface Society*, Coimbra, Portugal, 2001 (unpublished).
(27) Doi, M.; Edwards, S. F. *The Theory of Polymer Dynamics*; Oxford University Press: Oxford, U.K., 1986.
(28) Landau, D. P.; Binder, K. *A Guide to Monte Carlo Simulations in Statistical Physics*; Cambridge University Press: Cambridge, U.K., 2005.
(29) Hu, W. *J. Chem. Phys.* **1998**, *109*, 3686–3690.
(30) Guillot, S.; Lairez, D.; Axelos, M. A. V. *J. Appl. Crystallogr.* **2000**, *33*, 669–672.
(31) Rawiso, M. De l'intensité à la structure en physico-chimie des polymères. In *Diffusion de neutrons aux petits angles*; Cotton, J. P., Nallet, F., Eds.; EDP Sciences: France, 1999; Vol. 9.
(32) Baschnagel, J.; Binder, K. *Physica A* **1994**, *204*, 47–75.
(33) Higgins, J. S.; Benoît, H. C. *Polymers and Neutron Scattering*; Clarendon Press: Oxford, U.K., 1994.
(34) Nallet, F. De l'intensité à la structure en physico-chimie des milieux dispersés. In *Diffusion de neutrons aux petits angles*; Cotton, J. P.; Nallet, F., Eds.; EDP Sciences: France, 1999; Vol. 9.

MA801337A